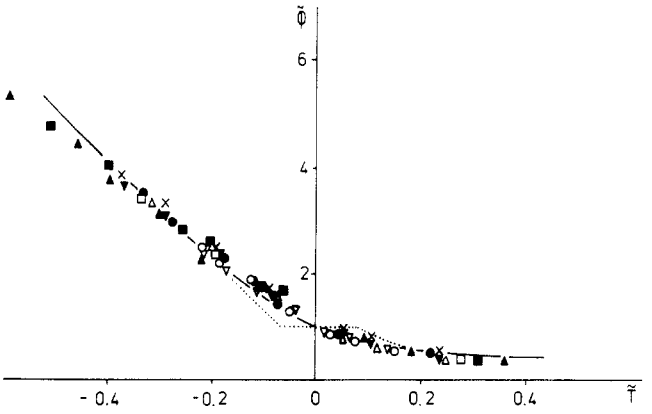

Figure 10. Comparison of theoretical results with the experiments. The solid line was calculated by eq 10.a, while the dotted one by eq 23. The values of the constants are given in the text.

thermal blob theories were considered. We have shown that the James–Guth theory exhibits scaling behavior. As a result of this, one can construct a universal function for the dependence of the scaled quantities. It has been shown that in the limiting cases the scaling functions belonging to either the James–Guth or the thermal blob theories coincide.

The Flory–Hermans–Wall–Kuhn theory gives basically different swelling behavior: below the Θ temperature a first-order phase transition is predicted and no scaling behavior has been observed.

Experimental results obtained for chemically cross-linked PVAc networks swollen to equilibrium in isopropyl alcohol are in agreement with the prediction of both James–Guth and thermal blob theories.

Acknowledgment. This research has been supported by AKA and OTKA grants (no. 1-3-86-229, no. 1204/86) of the Hungarian Academy of Sciences.

Registry No. (VA)(glutaraldehyde) (copolymer), 32630-65-2.

References and Notes

(1) Dušek, K.; Patterson, D. *J. Polym. Sci., Polym. Phys. Ed.* **1968**, *6*, 1209.
(2) Dušek, K.; Prins, W. *Adv. Polym. Sci.* **1969** *6*, 1.
(3) Tanaka, T. *Phys. Rev. Lett.* **1978**, *40*, 820.
(4) Khoklov, A. R. *Polymer* **1980**, *21*, 376.
(5) Ilavsky, M. *Polymer* **1981**, *22*, 1678.
(6) Janas, V. F.; Rodriguez, F.; Cohen, F. *Macromolecules* **1980**, *13*, 977.
(7) Aharoni, S. M.; Wertz, D. H. *J. Macromol. Sci., Phys.* **1983**, *B22*, 129.
(8) Zrinyi, M.; Molnár, T.; Horváth, E. *Polymer* **1981**, *22*, 429.
(9) Zrinyi, M.; Wolfram, E. *J. Colloid Interface Sci.* **1982**, *90*, 1.
(10) Zrinyi, M.; Horkay, F. *Macromolecules* **1984**, *17*, 2805.
(11) Zrinyi, M.; Wolfram, E. *Prog. Colloid Polym. Sci.* **1985**, *71*, 20.
(12) Erman, B.; Baysal, B. M. *Macromolecules* **1985**, *18*, 1696.
(13) Candau, S.; Munch, J. P.; Hild, G. *J. Phys. (Les Ulis, Fr.)* **1980**, *41*, 1031.
(14) Flory, P. J. *Principles of Polymer Chemistry*; Cornell University: Ithaca, NY, 1953.
(15) Van der Kraats, E. J.; Winkeler, M. A. M.; Potters, J. M.; Prins, W. *Recl. Trav. Chim. Pays-Bas* **1969**, *88*, 449.
(16) Froelich, D.; Crawford, D.; Rozek, T.; Prins, W. *Macromolecules* **1972**, *5*, 100.
(17) Pennings, A. J.; Prins, W. *Polym. Sci.* **1961**, *49*, 507.
(18) Rijke, A. M. *J. Polym. Sci.* **1966**, *4*, 131.
(19) Horkay, F.; Nagy, M. *Acta Chim. Hung.* **1984**, *115*, 305.
(20) Horkay, F.; Nagy, M.; Zrinyi, M. *Acta Chim. Acad. Sci. Hung.* **1981**, *108*, 287.
(21) de Gennes, P. G. *Scaling Concepts in Polymer Physics*; Cornell University: Ithaca, NY, 1979.
(22) Brochard, F. *J. Phys. (Les Ulis, Fr.)* **1979**, *40*, 1049.
(23) Candau, S.; Bastide, J.; Delsanti, M. *Adv. Polym. Sci.* **1982**, *44*, 27.
(24) Beltzung, M.; Herz, J.; Picot, C. *Macromolecules* **1983**, *15*, 1594.
(25) Bastide, J.; Picot, S.; Candau, S. *J. Macromol. Sci., Phys.* **1981**, *B19*, 13.
(26) Bastide, J.; Herz, J.; Boué, F. *J. Phys. (Les Ulis, Fr.)* **1985**, *46*, 1967.
(27) Daoud, M.; Jannink, G. *J. Phys. (Les Ulis, Fr.)* **1976**, *37*, 973.
(28) Akcasu, A. Z.; Han, C. C. *Macromolecules* **1979**, *12*, 276.
(29) Weill, G.; des Cloizeaux, J. *J. Phys. (Les Ulis, Fr.)* **1979**, *40*, 99.
(30) Horkay, F.; Zrinyi, M. *Macromolecules* **1982**, *15*, 1306.
(31) Horkay, F.; Zrinyi, M. *J. Macromol. Sci., Phys.* **1986**, *B25*, 307.
(32) Horkay, F.; Nagy, M. *Polym. Bull (Berlin)* **1980**, *3*, 457.
(33) Horkay, F.; Nagy, M. *Acta Chim. Acad. Sci. Hung.* **1981**, *107*, 321.

Gelation Process by Size-Exclusion Chromatography Coupled with Light Scattering

F. Schosseler,* H. Benoit, Z. Grubisic-Gallot, and Cl. Strazielle

Institut Charles Sadron (CRM-EAHP), CNRS-ULP, 6, rue Boussingault, 67083 Strasbourg-Cedex, France

L. Leibler

Laboratoire de Physico-Chimie Macromoléculaire, UA 278, ESPCI, 10, rue Vauquelin, 75231 Paris-Cedex 05, France. *Received December 8, 1987; Revised Manuscript Received June 13, 1988*

ABSTRACT: We study the sol–gel transition obtained by cross-linking of polymer solutions. We measure the size distribution function of diluted pregel samples by size-exclusion chromatography coupled with light scattering. With this technique a very good approximation of molecular weight distribution function is obtained although the separation criterion in the columns is the hydrodynamic volume of the molecules. Experimental results are found to be consistent with a scaling description of the sol–gel transition.

I. Introduction

Although polymeric gels are widely used materials, an extended comprehension of their properties is far from being reached. In particular, the relationship between the structure and the properties of gels is not yet clearly understood, even in neutral gels.[1-5] Probably this complicated relationship originates in the method of synthesis of the gels, in the very beginning of gel formation. Therefore, among the large amount of experimental and theoretical work on gels, particular attention has been paid to gel

0024-9297/89/2222-0400$01.50/0

synthesis and the so-called sol–gel transition,[1,2,6] i.e., the transformation of the viscous liquid in the reaction bath into a solid with an elastic behavior. In a chemical gel this transformation occurs through the reaction of small multifunctional units to form bigger ramified molecules. The viscosity of the reaction bath increases dramatically until a huge molecule spans the whole container. This is the gel point where the polydispersity is infinite: all molecular sizes from the precursor units to the infinite cluster size are present in the reaction bath. From this time, an elastic modulus appears that increases as the reaction goes on. The remaining sol phase is progressively incorporated into the gel phase, the largest clusters reacting the more rapidly.[1,6]

Since the first investigations by Flory and Stockmayer[1,7,8] both theoretical and experimental work on gelation try to understand the deep changes in macroscopic properties that occur in the reaction bath during the sol–gel transition. These changes reflect the evolution of the molecular weight distribution function of molecules in the reaction bath, which has been described by many different models.[1,6]

The interesting feature of these models is to introduce a scaling form of the distribution function of high molecular weight species. This is a fundamental point that implies a very simple relationship between all the moments of the weight distribution function. However, this scaling form is difficult to check through the evolution of a few moments of the size distribution function with advancement of the reaction: weight-average molecular weight, z-average radius of gyration or hydrodynamic radius of the molecules in the sol phase, gel fraction, etc. The difficulty arises mainly from the lack of accuracy in estimating the exact location of the gel point and the actual advancement of the reaction.

In this paper we give the details of a method we already proposed[9] to measure directly the size distribution function (sdf) of the molecules in the reaction bath. For this we use size-exclusion chromatography (SEC) to separate the sol phase into fractions according to their hydrodynamic volume. With a differential refractometer and a low-angle laser-light-scattering (LALLS) apparatus coupled on line with SEC columns we can measure the concentration and the average molecular weight of molecules in each fraction. However, the quantitative interpretation of the experimental data concerning large branched molecules is not straightforward. The use of this method to study gelation processes requires some precautions, and several conditions are to be met to get a meaningful size distribution function. The purposes of this paper are to analyze these conditions and to present the measurements of the size distribution functions for a particular gelation process, namely, cross-linking of polystyrene solutions by γ-irradiation. We have already studied this system by light scattering.[10] The SEC provides new interesting information on the process.

This paper is organized as follows: in part II, we recall briefly the basis of scaling description of sol–gel transition. Experimental details constitute part III. The determination of size distribution functions from SEC chromatograms is detailed in part IV together with the conditions to be met for a sensible calculation. The limitations of the method are also discussed. In part V, we give the results we obtained with our system.

II. Theoretical Background

From the very beginning, the most fundamental aspect of the sol–gel transition was recognized by Flory and Stockmayer:[1,7,8] if the chemical reaction between the species occurs at random, then the description of the system is greatly simplified and is insensitive to the particular details of the chemical system that is considered. Near the gel point the molecular weight distribution function (MWD) has a universal behavior for large branched molecules. When the functionality of the reacting units is large, the asymptotic form of the MWD is given by

$$\Phi(M,\epsilon) \sim M^{-3/2} \exp(-\tfrac{1}{2}M\epsilon^2) \tag{1}$$

where $\Phi(M)\,dM$ is the weight fraction of monomers belonging to molecules with molecular weight between M and $M + dM$, and $\epsilon = (p_c - p)/p_c$ is the distance to the gel point. Here p is the fraction of reacted bonds and p_c the value of p at the gel point.

However, the MWD (eq 1) was calculated assuming that the branched molecules have a treelike structure and that no excluded volume effects are present in the reaction bath.

More recently[11,12] it was argued that the sol–gel transition could be modeled by percolation theory, which allows one to take into account loop formation and steric effects in the branching process. Equation 1 is then modified to

$$\Phi(M,\epsilon) \sim M^{-\tau+1} f(M/M^*) \tag{2}$$

where $f(x)$ is a cutoff function that is of the order of unity for small x and that decreases very sharply for large x. M^* is a cutoff molecular weight that diverges at the gel point as

$$M^* \sim \epsilon^{-1/\sigma} \tag{3}$$

τ and σ are two critical exponents whose values are different in percolation theory ($\tau \simeq 2.2$, $\sigma \simeq 0.46$) and in the Flory–Stockmayer approach ($\tau = {}^5/_2$, $\sigma = {}^1/_2$). As a consequence of eq 2, the function $\Phi(M)$ has a simple algebraic decay at the gel point $\Phi(M) \sim M^{-\tau+1}$.[12] The cutoff function f takes into account crossover effects that are present when the system is not exactly at the gel point.

The scaling form (eq 2) allows one to calculate very easily all the moments of the distribution near the gel point. Since the kth moment is defined as $\langle M^k \rangle = \int M^k \Phi(M)\,dM$, it scales like

$$\langle M^k \rangle \sim M^{*k+2-\tau} \tag{4}$$

Thus for complete characterization of the sol phase near the gel point it is sufficient to measure the exponent τ and the cutoff size M^* (or equivalently ϵ and the exponent σ). Percolation theory predicts that eq 2 describes also the sol phase beyond the gel point.[12,13] The crossover function is of special interest because of its qualitatively different behavior in classical and percolation theory. In the first case, the asymptotic form derived from Stockmayer's distribution results in an exponentially decreasing function for positive values of the molecular weight, i.e.

$$f(M/M^*) \sim \exp(-M/2M^*) \tag{5}$$

On the other hand, results from numerical simulations show a maximum in $f(M/M^*)$ for a nonzero value of the reduced parameter. The numerical data are well described by a Gaussian curve:

$$f(z) \sim \exp(-(z - z_{max})^2) \tag{6}$$

with $z \sim (M/M^*)^\sigma$. This empirical equation seems to be valid on both sides of the gel point.[12,13]

This shows the interest of the study of pregel samples. In the case where the above description is correct, the results we get before the gel point give information on the evolution of the molecular weight distribution function

after the gel point, where the characterization of the sol phase is much more difficult to achieve.

III. Experimental Section

The gelation process and sample preparation have been already described in reference 10. The cross-linking of the polystyrene solution in cyclopentane is induced by ^{60}Co γ-irradiation. The concentration of polymer during cross-linking is $c = 0.1$ g/cm^3, and the weight averaged molecular weight of precursor chains is $M_w(0) \simeq 55\,000$ (polydispersity 1.2). The temperature during irradiation is kept to 22 ± 1 °C, which is slightly higher than the Θ temperature for the PS–C_5H_{10} system. The concentration c is close to the overlap concentration of the precursor chains. The gel point is obtained after an irradiation time of 10^5 min with an approximate dose rate of 1000 rad/min. All details of samples preparation have been given elsewhere.[10] The important point is that the advancement of the reaction is controlled by the irradiation dose.[26] Cross-linking comes about by combination of neighboring radicals on the chains. In polymer solutions these radicals can be formed in two distinct ways: direct radiolysis of the polystyrene[27] or transfer on the chains of the free radicals obtained in the radiolysis of the solvent.[28] Direct radiolysis of polystyrene in the melt produces both cross-linking ($G_c = 0.034$) and degradation ($G_d = 0.0034$) of the chains,[29] where G_c and G_d are respectively the number of cross-linking and chain scissions obtained for 100 eV absorbed by the matter. The transfer of radicals from the solvent induces no chain scission and is the dominant process in a polymer solution with polymer weight fraction around 0.1. Thus degradation of the polymer during the irradiation is strongly reduced: size-exclusion chromatography does not indicate such a degradation, which would be visible in the low molecular weight side of the chromatograms. In this study we consider only samples before the gel point. Once the desired irradiation dose is obtained, the samples are washed in toluene. The sol phase is then extracted by evaporation, dilution in benzene, and finally lyophylization. The final product is dried under vacuum at 50 °C and is ready for characterization by the usual physicochemical methods. Measurements of average molecular weights and radii of gyration by light-scattering experiments have already been reported.[10]

Here we use SEC coupled on line with a LALLS apparatus.[14] Measurements are performed in THF at 25 °C with a Waters 150 C chromatograph and Microstyragel columns (nominal pore size: 10^3, 10^4, 10^5, 10^6 Å). The elution rate is 1 mL/min.

Dilute solutions ($c \simeq 10^{-3}$ g/cm^3) of the samples are prepared and injected into the columns. Branched molecules are there separated according to their hydrodynamic volume:[15] molecules with small hydrodynamic volume can explore a great fraction of the porous voids in the columns and therefore need more time than bigger molecules to flow through the columns.

At the output of the columns there is a small-angle light-scattering photometer (Chromatix CMX 100) with a 10-μL scattering cell, the scattering volume being 0.04 μL when the scattering angle is about 6°. The incident light is supplied by a He–Ne laser ($\lambda = 6328$ Å). This particular scattering geometry gives no angular dependence of intensity scattered by molecules whose radius of gyration is less than 2500 Å.

The concentration in the scattering volume was typically of about 10^{-6} g/cm^3. Since for branched polymers of high molecular weight the second virial coefficient is weak even in a good solvent (about 10^{-5} cm^3/g for branched polystyrene in toluene[10]) we can neglect within a very good approximation intermolecular contribution to scattering intensity. Therefore the scattered intensity is proportional to the product of the concentration and of the weight-averaged molecular weight of molecules that are present in the scattering volume. Moreover we measure independently the polymer concentration with a differential refractometer, taking into account the dead volume between the photometer and the refractometer.

Both detectors give continuous signals. However, we record them in a discrete way at constant time intervals or equivalently at constant elution volume intervals. Figures 1, 2 and 3, 4 show respectively the refractometry and light-scattering chromatograms.

To obtain meaningful distributions from the chromatograms, one has to be sure that there is no retention of the molecules inside the columns. In fact, for each experiment, we verified that the

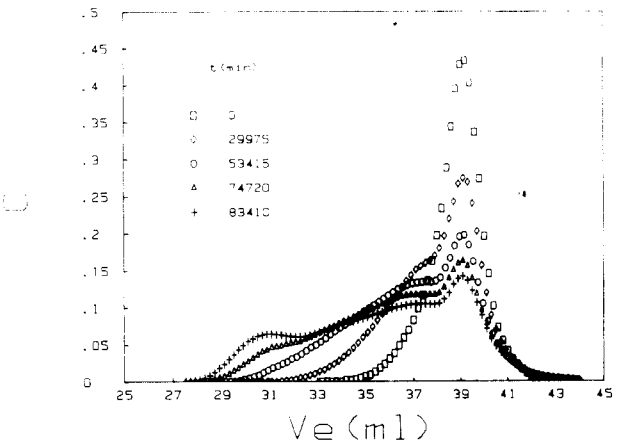

Figure 1. Refractometry chromatograms for samples with different irradiation time in minutes. The curves are normalized to a unit surface area.

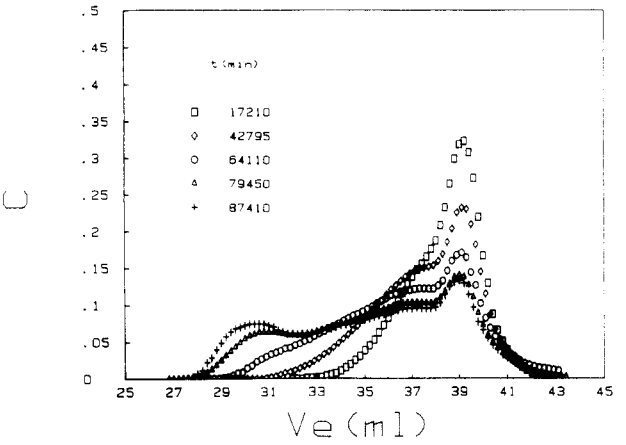

Figure 2. Same as Figure 1 with other samples.

amount of injected polymer and the area under the refractometry curve (Figures 1 and 2) were always in the same ratio.

Another difficulty is related to a possible degradation of molecules due to shear gradient effects. These effects are particularly important for large molecules and high flow rate of the solvent through the columns. As a result of this degradation the concentration of large molecules decreases while the fraction of molecules with intermediate molecular weight increases. This would lead to a drastic drop of the values of weight-averaged molecular weight. Since we obtain the same values for the molecular weight before and after SEC experiments (Figure 5), this degradation did not take place in our experiments. In fact, to minimize shear gradient effects, we used a low flow rate (1 mL/min) and we removed the prefilter, which is known to be responsible for the major part of the degradation process.[16] Also our branched molecules are much more compact than linear ones, and we can study higher molecular weights molecules without shear gradient effects becoming important.

Thus for the samples studied in this paper we found no indications of permanent retention or degradation in the SEC columns. This allows us to calculate significant size distribution functions from our data. However, the method is reliable for studying samples that are not too close to the gel point. For more highly irradiated samples we found that some molecules were retained in the columns and moreover the molecules with the highest molecular weights were no longer separated.

IV. Calculation of Size Distribution Functions

In the study of the sol–gel transition, the useful quantity is the molecular weight distribution function $\Phi(M,\epsilon)$. However, this function is not directly measured in a SEC experiment. This is for two main reasons. First, in the SEC columns the molecules are separated into fractions according to their hydrodynamical volume. Second, the

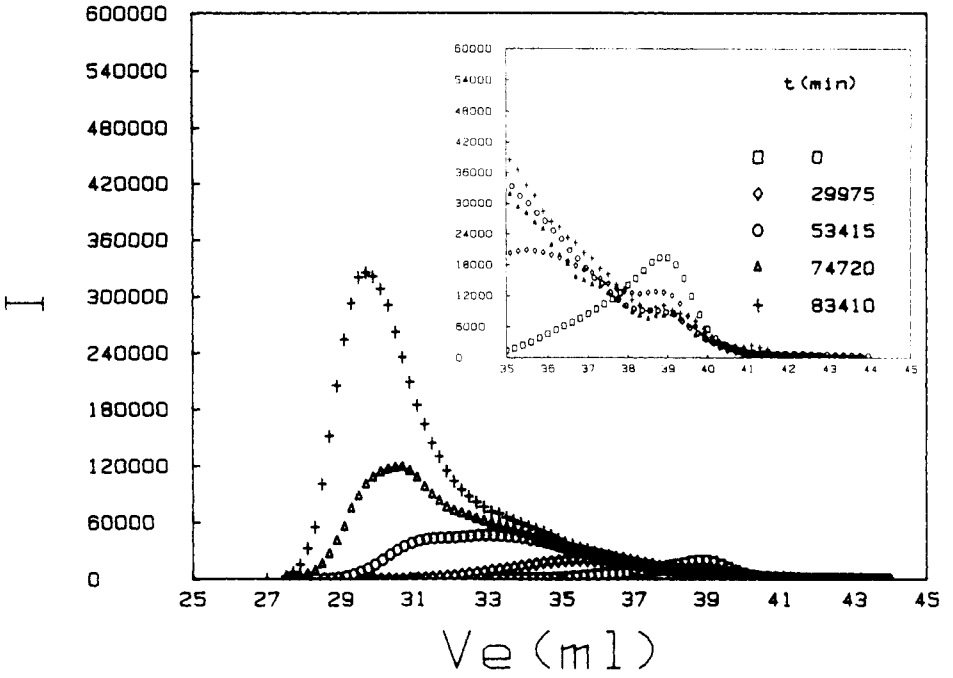

Figure 3. Light-scattering chromatograms of the samples in Figure 1. The curves are normalized so that surface area is proportional to the weight-average molecular weight of the samples. The inset magnifies the region corresponding to the linear precursor chains.

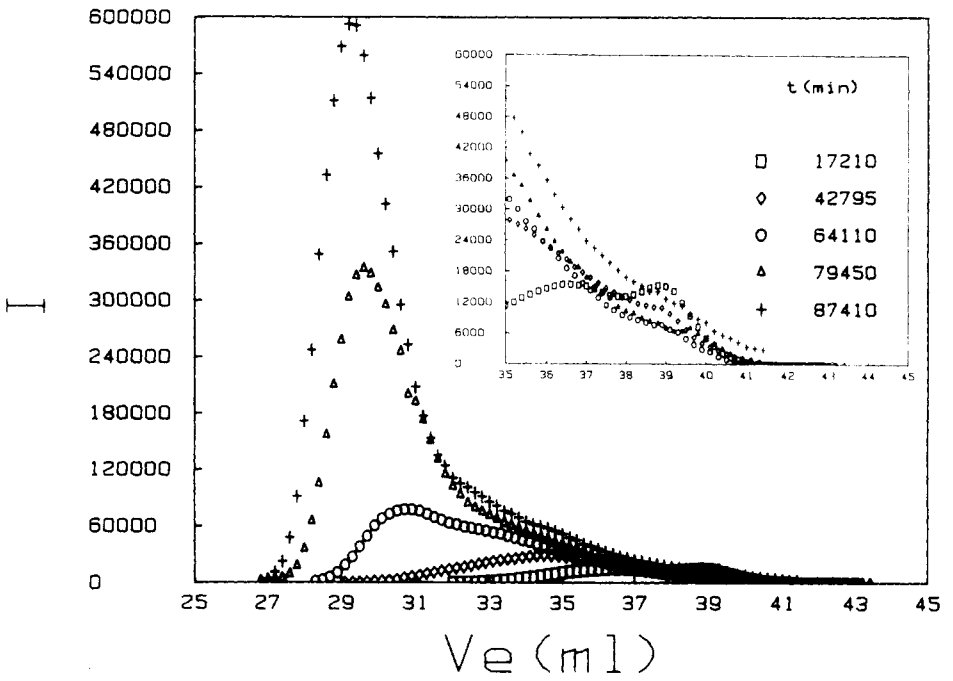

Figure 4. Same as Figure 3 for the samples in Figure 2.

elution volume v_e is not proportional to the hydrodynamic volume v_H. Instead we have[15]

$$\log v_H = k_1 - k_2 v_e \quad (7)$$

where k_1 and k_2 are two constants depending on the solvent and the columns.

We first note that the hydrodynamic volume of chains depends on their configuration and is a time-dependent quantity. In the following we will consider that during the separation process, the molecules can experience all their configurations so that they are well defined by their average hydrodynamic volume. It is this value that appears in eq 7. We will not consider thermodynamic fluctuations around this mean value.

The basic feature of the sol phase near the gel point is the large polydispersity. This includes not only molecular weight polydispersity but also shape polydispersity.[12] There are a number of molecules with the same molecular weight but different shapes, i.e., different hydrodynamic volumes. These molecules are eluted at different times, and thus in a given fraction a mixing of different molecular weights occurs. This effect is not to be confused with axial dispersion effects that result from the imperfections of the apparatus and are superimposed upon shape polydispersity effects.

It is difficult to estimate shape polydispersity effects because theories often are not able to describe the molecular weight distribution function of molecules with constant hydrodynamic volume. However, if branched molecules are self-similar objects, we can expect that the fluctuations of the size at a given molecular weight will grow like the size. This point can be illustrated in the

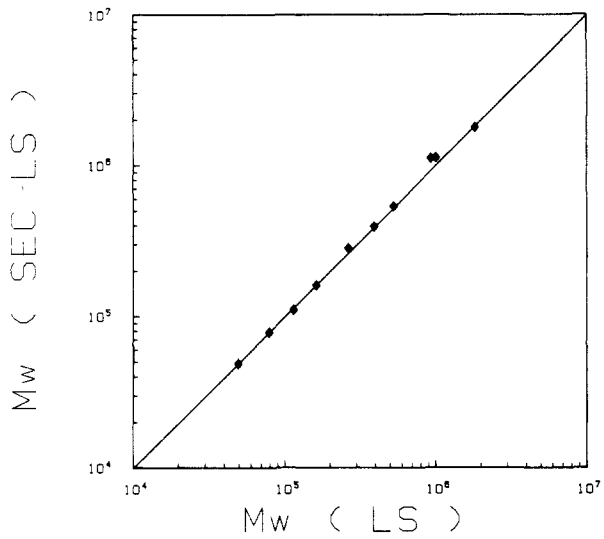

Figure 5. Comparison of weight-average molecular weights measured by static light-scattering M_w (LS)[10] and size-exclusion chromatography coupled with low-angle laser-light-scattering M_w (SEC-LS).

Table I
Average Size $\langle g \rangle$ and Fluctuations δ of the Average Size of Branched Molecules as Functions of the Number of Tetrafunctional Branch Units in the Zimm-Stockmayer Model[17] (See Text and Appendix A)

	no. of branch units						
	1	2	3	4	5	6	15
$\langle g \rangle$	0.8	0.690	0.618	0.567	0.525	0.493	0.345
δ	0.11	0.13	0.135				

simple Zimm-Stockmayer model for branched polymers.[17,21] In Appendix A, we give g, $\langle g \rangle$, and $\langle g^2 \rangle$ where g is the ratio of the radius of gyration R of a branched molecule to the radius of a linear one with same molecular weight. It is found that

$$(\langle g^2 \rangle - \langle g \rangle^2)^{1/2} = \delta(n,f)\langle g \rangle$$

where $\delta(n,f)$ depends only on the number n and the functionality f of the branch units (see Appendix A). We have summarized in Table I the results for molecules of functionality four. We find $\delta(1,4) \simeq 0.11$, $\delta(2,4) \simeq 0.13$, $\delta(3,4) \simeq 0.135$. Assuming $V_1 \sim R^3$ we can then estimate from the calibration curve of (7) the dispersion in elution volume that results from the shape polydispersity at constant molecular weight:

$$\Delta v_e \simeq \frac{3}{k_2}\frac{\Delta R}{R} \tag{8}$$

With typical values, $\Delta R/R \simeq 0.15$ and $k_2 \simeq 0.3$ mL^{-2} (Figure 8), we obtain $\Delta v_e \simeq 1.5$ mL. We note that due to the particular relationship between elution volume and hydrodynamic volume, the broadening does not depend on the elution volume.

Axial dispersion effects are responsible for an additional broadening of the chromatograms. Even a polymer sample with a unique and well-defined hydrodynamic volume will not be eluted as a δ function but rather as a Gaussian curve with a half-width σ_a. This broadening is due to the imperfections of the apparatus. Depending on the apparatus and the way it is measured, σ_a is found to be either dependent[18] or independent[19] of the elution volume. A typical order of magnitude for σ_a in the columns we used is $\sigma_a \simeq 0.75$ mL.

Now we assume that shape distribution effects change the chromatogram of a single molecular weight fraction from a δ function to a Gaussian curve with half-width Δv_e (eq 8). Combining these with axial dispersion effects, we obtain a Gaussian chromatogram with half-width $\Sigma = (\sigma_a^2 + \Delta v_e^2)^{1/2}$, with $\Sigma = 1.6$ mL as a typical order of magnitude. This means that the molecular weights of the molecules that are present in a given fraction can be very different.

However, it is still possible to obtain a very good approximation of the molecular weight distribution function by the following procedure. First we divide the chromatograms into fractions with the same width Δv. Then for each fraction i we calculate the areas R_i and I_i under the refractometry and light scattering curves, respectively. I_i is proportional to the intensity scattered by the molecules with elution volume between v_i and $v_i + \Delta v$, while R_i is proportional to their concentration. The weight fraction f_i of these molecules and their weight-average molecular weight $\bar{M}_i$ are then given by

$$f_i = R_i/\sum_i R_i$$

$$\bar{M}_i = kI_i/R_i \tag{9}$$

where k is a known apparatus constant. We have the conditions $\sum f_i = 1$ and $\sum f_i \bar{M}_i = M_w$, where M_w is the total weight-average molecular weight of the sample. Now from f_i and $\bar{M}_i$ we can obtain easily the cumulative weight distribution function $F(\bar{M}_j)$ defined as usually by

$$F(\bar{M}_j) = \sum_{i=1}^{j} f_i \tag{10}$$

We then define the size distribution function $\Phi(M)$ through

$$F(\bar{M}_j) = \int_0^{\bar{M}_j} \Phi(M)\, dM \tag{11}$$

Thus the function $\Phi(M)$ is simply obtained from the numerical differentiation of the cumulative weight distribution function $F(\bar{M})$.

The latter step, i.e., differentiation, is very important to get a meaningful size distribution function. Such a distribution function has the following properties:

$$\int \Phi(M)\, dM = 1$$

$$\int \Phi(M) M\, dM = M_w \tag{12}$$

Note that in eq 12 the integration is performed over molecular weight. Often in the literature the quantity $f_i(\bar{M}_i)$ is called weight distribution function although it does not verify (12). Instead we have

$$\int f_i(\bar{M}_i)\, dv_i = 1$$

$$\int f_i(\bar{M}_i)\bar{M}_i\, dv_i = M_w \tag{13}$$

where the integration is taken over elution volumes. Because of the nonlinear relationship between molecular weight and elution volume, the functions $f_i(\bar{M}_i)$ and $\Phi(M)$ are not equivalent. For comparison with gelation theories we have to use the function $\Phi(M)$.

In Appendix B, we simulate chromatograms from Stockmayer's distribution function[8] and compare the calculated $\Phi(M,\epsilon)$ with the input distribution function. We find they are in a good agreement.

One point that should be important is the size Δv of the fraction. It is clear that Δv must remain small compared to the total spread of the chromatograms to describe the details of the curves. In the opposite way, we find in the

simulations that Δv can be as small as we want. Even if we simply take for R_i and I_i the values of the refractometry and light-scattering curves (i.e., without integration), we still recover a good approximation of the input size distribution function.

However, in a real experiment, some noise can be present in the chromatograms and, moreover, errors are possible in the measurements of the dead volume between the detectors. Therefore it is better to give a finite value to Δv and to keep the integration procedure. We found that a very efficient way to proceed in usual situations is the following.

First, give a small value to Δv to have a great number of experimental points and perform the integration to get I_i and R_i.

Then in each point i, calculate the mean values:

$$\bar{M}_i = k \sum_{j=i-p}^{i+p} I_j / \sum_{j=i-p}^{i+p} R_j$$

$$f'_i = \sum_{j=i-p}^{i+p} f_j/(2p+1) \tag{14}$$

with p between 0 and 3, according to the noise in the chromatograms. By this procedure we eliminate the experimental scattering, keeping the same number of experimental points. The general shape of the function $\Phi(M)$ remains unaffected by this procedure, although it becomes smoother. In our experiments, Δv was typically 0.2 mL and p was 2 or 3.

V. Picture of Gelation of Chains through SEC-LALLS Experiments

Measurement of Typical Cluster Size. From the chromatograms in Figures 1–4 we can get directly a nice qualitative picture of the gelation process.

The signal at the output of the differential refractometer is simply proportional to the monomer concentration in the eluted fraction. We see that as the irradiation time increases and the cross-linking reaction proceeds, the concentration of monomers belonging to the linear precursor chains decreases. These chains are cross-linking, building up larger molecules that appear as the wing in the small elution volumes side of the peak.

On the other hand, since the signal obtained through the light-scattering apparatus (Figures 3 and 4) is proportional to the product of the molecular weight and concentration of eluted molecules, we see immediately that the small wing in the refractometry curve indeed corresponds to branched molecules with high molecular weights. Although they are present in small quantities, their contribution in the light-scattering chromatograms is very important. In fact, for most of the samples, the contribution of high molecular weight molecules to scattered intensity is much larger than that due to the linear precursor chains although the latter are still the more abundant species (Figures 1–4). The same feature can be observed on the simulated chromatograms (Figure 12) we give in appendix B.

This experimental behavior agrees quite well with the typical cluster size picture which lies behind the scaling description of the sol–gel transition.[12,13] This typical size is the cutoff molecular weight M^*, which enters into the cross-over function f. Since the kth moment of the distribution is given by $\langle M^k \rangle = \int M^{k+1-\tau} f(M/M^*)\, dM$, the integrand is the product of a monotonously increasing function (for $k > \tau - 1$) and a cutoff function that decreases more rapidly than any power law for molecular weights larger than the cutoff M^*. Thus clusters with molecular weight around M^* give the largest contribution to the integral. This is the physical basis for eq 4.

Figures 3 and 4 are beautiful illustrations for this behavior and provide us with an experimental measure of the typical size M^* of the samples. We simply identify M^* with the molecular weight of the fraction that gives the largest contribution to the scattered intensity. In the case where one could know precisely ϵ, the relative distance to the gel point, this would allow a direct measure of the exponent τ, which gives the divergence of the typical cluster size. However, in our case, we cannot measure the advancement of the reaction. Nevertheless, we can obtain the exponent τ directly through the M^* dependence of the weight-average molecular weight M_w:

$$M_w \sim \langle M \rangle \sim M^{*3-\tau} \tag{15}$$

A least-squares fit through the data shown in Figure 6 gives $\tau = 2.3 \pm 0.1$.

One point should be made concerning the maximum observed in the light-scattering chromatograms. Strictly speaking, there is no dominant contribution in the terms that enter into the calculation of the weight-average molecular weight since M_w corresponds to the first moment ($k = 1$) of the size distribution function Φ and $\tau \simeq 2.3$: $M^{k+1-\tau} f(M/M^*)\, dM$ is a monotonously decreasing function when $k = 1$.

However, as mentioned in section IV, the intensity scattered by a given fraction is

$$I_i = k \int_{M_i}^{M_{i+1}} M\Phi(M)\, dM \simeq k M_i \Phi(M_i)(M_{i+1} - M_i)$$

which we can approximate, using the calibration curve (7):

$$I_i \simeq M_i^2 \Phi(M_i) \Delta v \tag{16}$$

since the width Δv of the fraction is kept constant. This explains the maximum that is observed in the light-scattering chromatograms. Correspondingly the refractometer curves should not exhibit a maximum since

$$R_i = \int_{M_i}^{M_{i+1}} \Phi(M)\, dM \simeq M_i \Phi(M_i) \Delta v$$

For very high molecular weights, when we approach the columns exclusion volume, the calibration curve (7) is no longer valid and a maximum can appear even in refractometer curves. In this case M^* measured from light-scattering data no longer corresponds to the maximum contribution to the second moment of the distribution as in eq 16.

Once we have calculated the size distribution $\Phi(M)$ according the procedure described in section IV, we can also determine a cutoff molecular weight simply by evaluating the term $M^2\Phi(M)$ for all experimental data points in a sample. The maximum value should in principle correspond to the same characteristic size as M^*. For our samples we verified that the two procedures give similar values. However, in the following we shall use only the value M^* determined directly from the maximum in the experimental light-scattering chromatograms. In fact this value is less sensitive to experimental and numerical errors.

Conformation of Randomly Branched Molecules. Our experiments provide us with two different estimations of the swelling of the branched molecules in a good solvent.

In fact the typical cluster size is directly related to the z-average radius of gyration, defined by

$$\langle R_g^2 \rangle_z \simeq \frac{\int \Phi(M) M^2 M^{2\nu_b}\, dM}{\int \Phi(M) M^2\, dM} = \frac{\langle M^{2\nu_b+2} \rangle}{\langle M^2 \rangle} \tag{17}$$

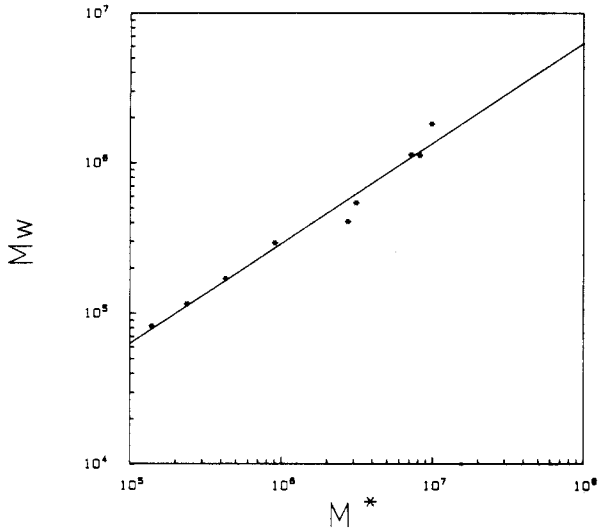

Figure 6. Variation of weight-average molecular weight M_w as a function of the characteristic size M^*. The slope of the continuous line is equal to $3 - \tau$ (eq 15).

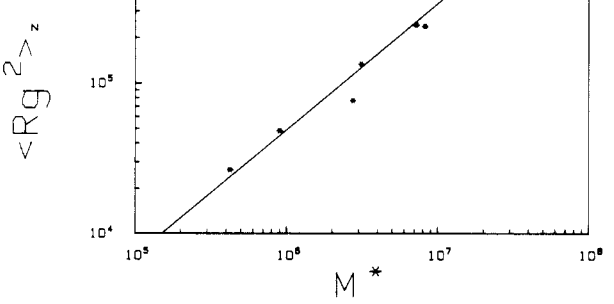

Figure 7. Variation of z-average radius of gyration[10] as a function of the characteristic size M^*. The continuous line has a slope $2\nu_b$ (eq 18).

where ν_b is the swelling exponent for randomly branched chains. Use of eq 4 leads to

$$\langle R_g^2 \rangle_z \simeq M^{*2\nu_b} \tag{18}$$

In Figure 7 we have plotted the values of $\langle R_g^2 \rangle_z$ in our samples[10] as a function of M^* values measured above. Scattering of the data is rather important for the two quantities obtained from different measurements. In fact, for SEC experiments we cannot use molecular weight samples that are too high, while for light-scattering experiments, the errors on the radii of gyration are larger for the smaller molecular weight samples. Therefore we have only a limited number of samples that match the two requirements. The value of ν_b corresponding to the straight line in Figure 7 is $\nu_b = 0.42 \pm 0.1$. However, here we want not to obtain an accurate value for ν_b but rather to show that the variation of $\langle R_g^2 \rangle_z$ as a function of M^* is compatible with eq 18.

A much more precise value for ν_b is obtained from the calibration curves we obtain from SEC experiments. Molecules are separated in the SEC columns according to their hydrodynamic volume: in eq 7, the constants k_1 and k_2 are dependent on the columns, the solvent, the flow rate, and the temperature, but they are the same for linear and branched molecules.[15] On the other hand, if we use a plot of the logarithm of the molecular weight as a function of the elution volume, the calibration curves will depend on the architecture of the molecules. This is shown in Figure 8 where we plot calibration curves for the linear precursor

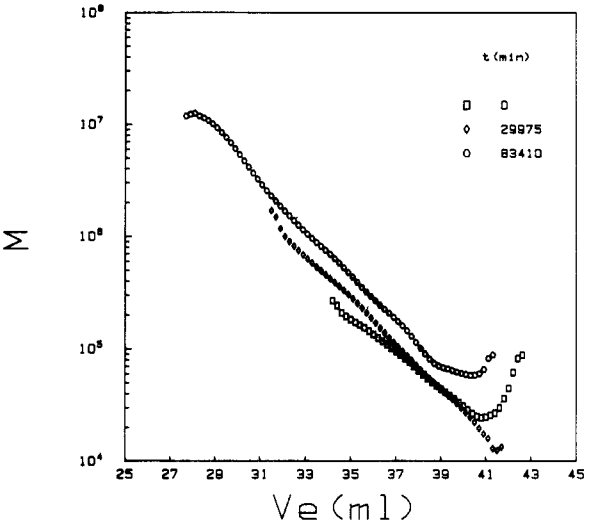

Figure 8. Calibration curves log $M = f(v_e)$ for the linear precursor chains ($t = 0$) and two branched samples. The slope of the curves are related to the swelling exponent of the molecules in a good solvent (see text).

chains and two branched samples. Following eq 7 and writing that the hydrodynamic volume of a molecule is proportional to the third power of its radius of gyration,[30] we find that

$$a_l/a_b = \nu_b/\nu_l \tag{19}$$

where a_l (a_b) and ν_l (ν_b) are the slope of calibration curve (in Figure 8) and the swelling exponent for linear (branched) molecules. Using the value $\nu_l \simeq 0.59$, we obtain from our data

$$\nu_b \simeq 0.49 \pm 0.03$$

which is very close to the theoretical value ($\nu_b = {}^1/_2$) expected for branched molecules in a good solvent.[20,21]

Scaling Behavior of the Size Distribution Function. The evolution of the size distribution function (sdf) $\Phi(M)$, obtained as explained in section IV, is shown in Figure 9 for several samples with different advancement of the cross-linking reaction.

Some qualitative features can be drawn from Figure 9. The peak observed in low molecular weight region ($\simeq 5 \times 10^4$) corresponds to linear precursor chains. Their concentration decreases during the reaction as they cross-link to form larger branched molecules. These large molecules are responsible for a huge increase in the spread of the sdf. In the linear chains sample the molecules have molecular weight below 3×10^5. In the irradiated samples we can observe clusters with molecular weights larger than several millions.

For intermediate molecular weights, the sdf decays algebraically with molecular weight, while for higher molecular weights $\Phi(M)$ decreases very rapidly. The extent of the algebraic decay region increases progressively as the weight-average molecular weight M_w of the sample increases.

This picture is consistent with a scaling form for the sdf. The increase in the spread of the sdf and the corresponding increase of the extent of the algebraic region are due to a shift of the cutoff molecular weight to higher values as the reaction proceeds. Moreover the slope measured in the algebraic decay region is consistent with the value of τ that is obtained from the M^* dependence of M_w.

We now want to perform a more quantitative test for scaling. However, for any numerical fit of the sdf we would have to postulate an analytic form for the crossover function $f(x)$. Here we prefer to use a quantitative test

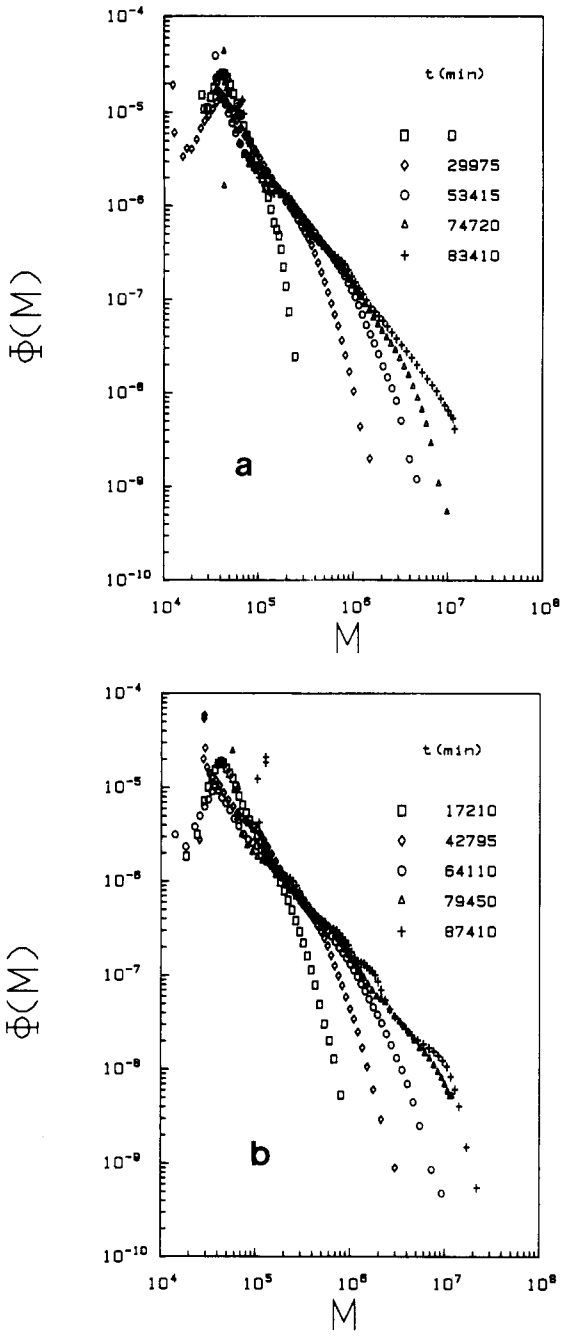

Figure 9. Size distribution functions calculated as explained in section IV: (a) samples of Figures 1 and 3; (b) samples of Figures 2 and 4.

that does not involve any a priori guess for $f(x)$.

From the experimental value $\Phi(M)$ and M^* measured for each sample, we build a new function[9] $G(M/M^*) = M^{*\tau-1}\Phi(M)$. According to eq 2, a plot of $G(M/M^*)$ as a function of the reduced molecular weight M/M^* should lead to a master curve that is independent of the advancement of the reaction. The reduced data are shown in Figure 10, and they collapse quite well on a unique curve. It is to be noted that we used for the exponent τ the experimental value determined from the M^* dependence of M_w. Thus to obtain the data collapse in Figure 10, we used no fitting parameters but only experimentally measured values. This test is rather severe since our experimental characteristic sizes vary by nearly 2 orders of magnitude.

It should be noted that, in Figure 10, samples with different advancement of the reaction contribute in different M/M^* range. In fact for very high molecular

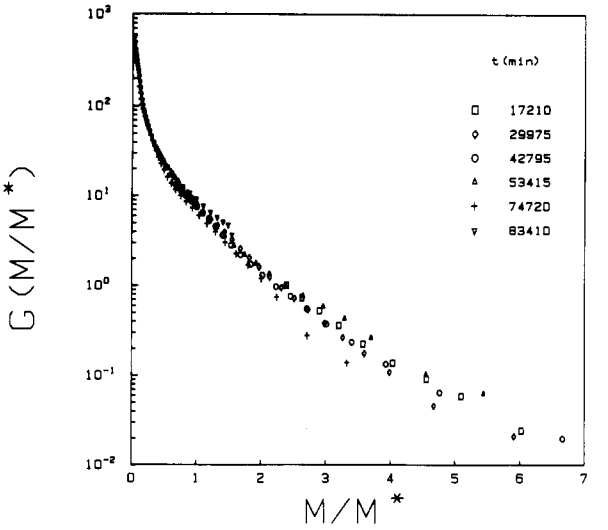

Figure 10. Renormalized size distribution functions $M^{*\tau-1}\Phi(M) = G(M/M^*)$ collapse on a unique curve when plotted as a function of M/M^*. M^*, M, τ, and $\Phi(M)$ are experimental quantities. No fitting parameter is used (see text).

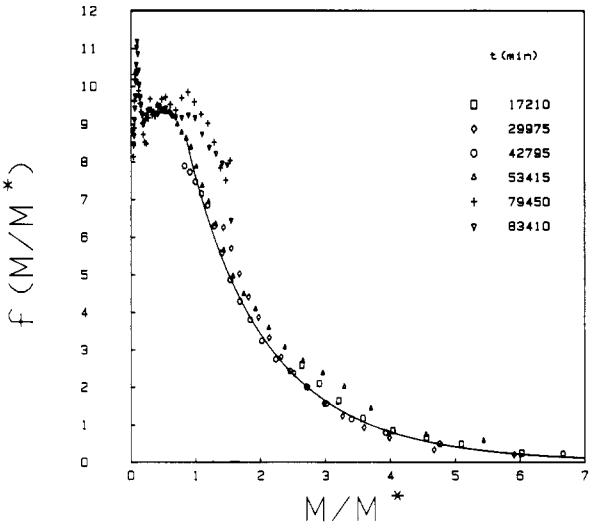

Figure 11. Crossover function $f(M/M^*) = M^{\tau-1}\Phi(M)$ as a function of M/M^* on linear scales. Solid line corresponds to $f(x) = 21.1 \exp(-x^{\zeta})$ with $\zeta = 0.85$.

weights, size-exclusion chromatography no longer separate molecules according to their hydrodynamic volume. Also some retention of very large molecules inside the columns may be observed. This prevents the characterization of very high molecular weights. For the more highly irradiated samples, the sdf cannot be measured far beyond the cutoff molecular weight M^*. The points for these samples correspond to values of $M/M^* \lesssim 1$. The points at higher values of M/M^* are obtained from the less highly irradiated samples. For all samples we have removed the points corresponding to molecular weights smaller than 3×10^5, i.e., the upper limit for the molecular weight of linear precursor chains.

Crossover Function. One step further we can attempt to get some information about the shape of the cutoff function $f(x)$. In numerical simulations it is obtained as the ratio of the sdf at a given advancement of the reaction to the same quantity at the gel point to eliminate numerical constants in eq 2. However, in our experiments we cannot measure the sdf at the transition. Therefore we obtain $f(M/M^*)$, apart from a numerical factor, by multiplying the experimental sdf $\Phi(M)$ by $M^{\tau-1}$ for each point. The results are shown in Figure 11 for several

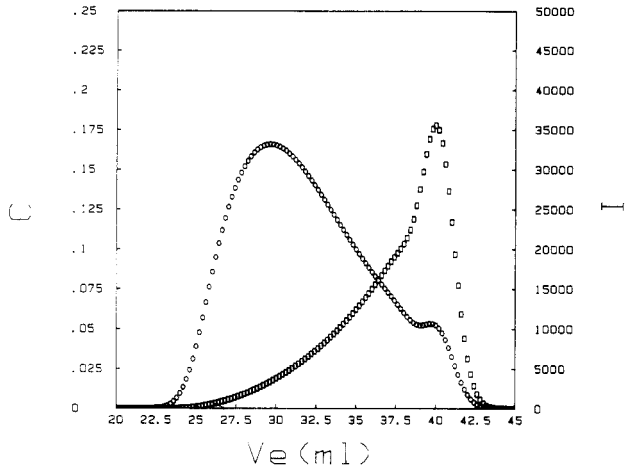

Figure 12. Chromatograms simulated from Stockmayer's distribution function at $\epsilon = 0.15$ and with a peak width $\Sigma = 1$ mL. The chromatograms are the superposition of 170 peaks (see Appendix B): (□) refractometry; (○) light scattering.

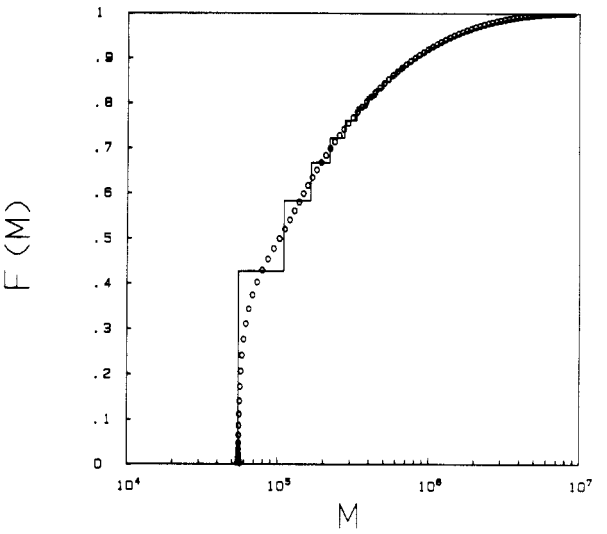

Figure 13. Cumulative weight distribution function obtained from the simulated data in Figure 12. Solid line corresponds to the input Stockmayer's weight distribution function.

samples, as a function of the reduced variable M/M^*.

In this representation we obtain again the collapse of the experimental points on a unique curve, although they appear more scattered than in Figure 10. In fact the calculation of $M^{\tau-1}\Phi(M)$ introduces errors, different for each point, on both M and $\Phi(M)$. On the other hand, in Figure 10 the calculation of $M^{*\tau-1}\Phi(M)$ involves for each sample only a constant error on M^*, apart from the error on $\Phi(M)$.

Moreover the representation we use enhances experimental errors for small values of the reduced parameter M/M^*, when the crossover function is still near unity.

Nevertheless the collapse on a unique curve is not so bad, except for a few samples. In fact, no adjusting parameter is used in Figure 11, and the data are obtained from graphical evaluation of the chromatograms. Computer-monitored data input is now available on the apparatus and will constitute a significant improvement in further experiments.

Taking into account the scattering of data points, we can make a few remarks.

First, it is not possible to decide whether or not the cutoff function has a maximum as in percolation theory[13] or is a monotonously decreasing function as in Flory–Stockmayer approach.[8] This is because we have poor accuracy for values of M/M^* smaller than 1: as in Figure 11, data points in this region come from high molecular weight samples, for which measurements of M^*, M and $\Phi(M)$ are less reliable.

If we now turn to the $M/M^* > 1$ region, the data do not seem compatible with either eq 5 or 6. In fact if we adjust constants to make 5 and 6 fit the data in the $1 < x < 3$ region, we find that, for high x values, these functions decrease too rapidly to describe the data in the $x > 3$ region. Instead we find that the choice

$$f(x) \simeq \exp(-x^{\zeta}), \quad x > 0.8 \tag{20}$$

describes rather well the data if we take the value $\zeta \simeq 0.85 \pm 0.05$ (continuous line in Figure 12).

Theoretical justification of eq 20 is not easy. Apart from an experimental artifact that could change the value of ζ in eq 5 from $\zeta = 1$ to $\zeta = 0.85$, we could think of eq 6 with a very small value for x_{max}: in this case, for $x > 1$, ζ would be given by $\zeta = 2\sigma$, which is compatible with the value of σ in percolation theory. In both cases, the behavior in the small M/M^* region is not correctly described. Thus it is not possible to get here a definite idea on the crossover function.

VI. Conclusions

In most cases, size-exclusion chromatography coupled on line with small-angle light scattering was considered as a rapid and convenient way to obtain weight-average molecular weights of polymer samples. In fact, using this apparatus, we can avoid frequently calibrating the columns with standards. Moreover, it was often thought of as a convenient way to observe the occurrence of aggregates or to get some idea of polydispersity, expressed as a ratio of two moments of the weight distribution function.

In this paper we showed that it is possible to go beyond this limited use. In fact the SEC-LALLS allows a very good quantitative determination of the size distribution function itself. Although the separation process occurs according to the hydrodynamic volume of molecules, we can calculate the size distribution function $\Phi(M)$ with the procedure we described. Thus it is possible to study accurately various problems, such as kinetics and mechanisms of chemical reactions[22] in polymer science or irreversible aggregation and gel formation, since we obtain directly the function of interest in the description of these phenomena.

Here we focused on the particular problem of gelation of solutions of linear chains. Even in this case, where shape polydispersity effects are superimposed upon axial dispersion effects, simulations show that the calculation of the size distribution function remains possible.

Moreover the size-exclusion chromatography technique allows a direct measurement of the characteristic size M^*, which is the basic concept underlying the scaling description of the sol–gel transition. This characteristic size is a measure of the effective advancement of the reaction. The knowledge of this quantity is particularly important in systems where the advancement of the reaction cannot be measured. The characteristic size M^* diverges at the gel point, where the polydispersity of the reaction bath becomes infinite. The divergence of all moments of the weight distribution function is very simply correlated to the behavior of M^*, due to the scaling form of the weight distribution function.

The variation of weight-average molecular weight M_w of sol molecules, as a function of M^*, allows the determination of the exponent τ, which describes the decay of the size distribution function at the gel point.

Similarly the variation of the z-average radius of gyration of sol molecules with M^* gives an estimation of the swelling

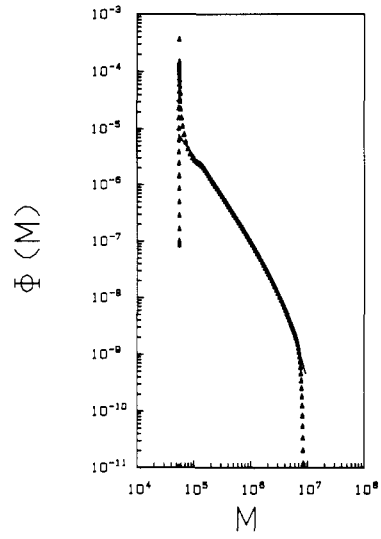

Figure 14. Size distribution function calculated from the cumulative weight distribution function in Figure 13. The agreement with the solid line corresponding to the input Stockmayer's distribution is very good except at the ends of the distribution (see Appendix B).

exponent ν_b of randomly branched molecules in a good solvent. A more precise value for ν_b can be obtained from the comparison of calibration curves log $M = f(v_e)$ for branched and linear molecules.

Using M^* as a renormalization parameter, we showed that the size distribution function indeed has a scaling form, consistent with the above experimental findings. Moreover it is possible to get an empirical analytic expression for the crossover function that modifies the power law behavior of the size distribution function when the system is not at the critical point.

The measured values $\tau = 2.3 \pm 0.1$ and $\nu_b = 0.49 \pm 0.03$ are in agreement with those obtained on the same system by light-[10] and neutron-scattering[23] techniques. Moreover they are consistent with experiments performed on different systems.[24,25]

In view of the data, a percolation picture of the gelation of chains appears to be plausible, and the influence of loops on the conformation of diluted molecules seems negligible. However, the crossover function in our system is not described by current theories, except for a possible complicated experimental artifact.

As a final conclusion, we note that SEC-LALLS is a very powerful tool to study growth processes in polymer science. Indeed, compared to other techniques, a lot of information can be obtained within a short time since a typical duration time for an experiment is less than 1 h. Moreover it can be easily applied to other systems.[25]

Acknowledgment. We gratefully acknowledge A. Lapp and B. Girard for kindly synthesizing for us the linear precursor chains as well as for advice at various experimental steps.

Appendix A: Size Fluctuations in the Zimm-Stockmayer Model[17]

The calculation of the dimensions of branched molecules can be achieved within the simple Zimm-Stockmayer (ZS) model, which assumes ideal Gaussian statistics for the chains and treelike structure for the molecules (no loops).

The quantity g is defined as usual by the ratio of radius of gyration of a branched molecule to the radius of gyration of a linear chain with the same molecular weight.

Clearly the maximal value for g is obtained when the chains are attached by the ends and $g_{max} = 1$. The minimal value for g corresponds to a compact star molecule containing $2n$ branches with $N_0/2$ statistical units. Then g_{min} is obtained through eq 16 of ZS:[17]

$$g_{min} = \tfrac{3}{2}n - \tfrac{1}{2}n^2$$

To calculate an average value, the distribution of branch units must be specified. ZS consider that for a molecule with given molecular weight and number of branch units, all possible arrangements of chains of varying lengths occur with the same frequency, provided the total number of units remains constant.

For molecules with one to three f functional branch units, the average values $\langle g \rangle$ are given by eq 15a, 18, and 19 (of ZS) averaged by using eq 21 of ZS. The average value $\langle g^2 \rangle$ is obtained in the same way.

Final results are as follows:

for one branch unit

$$\langle g \rangle = \frac{6f}{(f+1)(f+2)}$$

$$\langle g^2 \rangle = 36f!\frac{f^3 + 10f^2 + 13f - 4}{(f+5)!}$$

for two branch units

$$\langle g \rangle = 3\frac{5f^2 - 6f + 2}{f(4f^2 - 1)}$$

$$\langle g^2 \rangle = 9\frac{13f^4 + 28f^3 - 41f^2 + 2f + 8}{f(f+1)(f+2)(2f+3)(4f^2-1)}$$

for three branch units

$$\langle g \rangle = 2\frac{13f^2 - 20f + 8}{f(9f^2 - 9f + 2)}$$

$$\langle g^2 \rangle = 36\frac{(175f^4 - 12f^3 - 385f^2 + 274f - 32)(3f-3)!}{(3f+3)!}$$

where f is the functionality of the branch units.

We define $\delta^2(n,f) = (\langle g^2 \rangle - \langle g \rangle^2)/\langle g \rangle^2$, where n is the number of branch units. For high f we find $\delta(1,f) \simeq 1/f^{1/2}$ but $\delta(2,f) \simeq 0.2$ and $\delta(3,f) \simeq 0.19$. With $f = 4$, $\delta(1,4) \simeq 0.11$, $\delta(2,4) \simeq 0.13$, $\delta(3,4) \simeq 0.135$.

For a large number of four-functional branch units, the average value $\langle g \rangle$ can still be calculated, but computing $\langle g^2 \rangle$ becomes rather difficult. The results for $f = 4$ are summarized in Table I.

The quantity δ can also be calculated with a different formalism but by keeping the same approximations as ZS. Daoud and Joanny[21] have performed the calculation of δ for a mixture of tri- and difunctional units. They found in the high branching limit $\delta(n \gg 1,3) \simeq 0.137$.

No model is available to calculate the dimensions of branched molecules obtained by the cross-linking of preexisting chains with fixed length. Clearly the averages as performed in the ZS model are not adequate to describe a vulcanization process. However, we search only for qualitative results, and probably the trends remain the same as in the ZS model. The important point is that the quantity δ does not decrease but tends to a constant value for a large number of cross-links.

The exact value of the quantity δ is an open question. We can take it of the same order of magnitude as $\delta(n \gg 1.3) \simeq \delta(3,4)$ since we do not explicitely consider the numeric constants in eq 8.

Appendix B

In this appendix we want to show that the procedure we described in section IV is efficient to calculate the size distribution functions. For this purpose we use simulated

chromatograms and compare the calculated size distribution function with the input molecular weight distribution function.

The molecular weight distribution function was obtained by using Stockmayer's distribution for vulcanization. For the sake of simplicity we consider only the case where linear precursor chains are monodisperse, containing all N_0 monomers with molecular weight $m = 100$. Then, the weight fraction of monomers belonging to molecules containing n precursor chains is

$$\Phi(n,p) = nN_0p^{n-1}(1-p)^{N_0n-2n+2}\frac{(N_0n-n)!}{n!(N_0n-2n+2)!} \quad \text{(B1)}$$

In the example we show below, we used $N_0 = 550$ and a value p corresponding to a relative distance to the gel point $\epsilon = 0.15$. We recall that for vulcanization, we have $p_c = 1/(N_0 - 1)$. These conditions correspond for the sample to a weight-average molecular weight $M_w \simeq 3.5 \times 10^5$ and a characteristic size $M^* \simeq 2.2 \times 10^6$. It is to be noted that to describe correctly the sample, we had to consider molecules containing up to 170 linear chains. This can be seen by verifying the normalization of the function $\Phi(n,p)$, i.e., the condition

$$\sum_{n=1}^{N}\Phi(n,p) = 1$$

is fulfilled if N is sufficiently large. This illustrates the enormous spreading of the size distribution function as the gel point is approached.

In a second step, we calculate the elution volumes corresponding to the molecular weights nmN_0 of the branched molecules, using the calibration law

$$V_e(nN_0m) = V_0 - (1/k)\log n \quad \text{(B2)}$$

with V_0 being the elution volume of the linear chains. We used $V_0 = 40$ mL and $k = 0.15$ mL^{-1} for the example.

We then calculate the refractometry and light-scattering curves in L equidistant points, separated by ΔV, using the amplitudes (B1), smeared by a Gaussian factor:

$$R_i = \sum_{n=1}^{N}\frac{1}{(2\pi\Sigma)^{1/2}}\exp\left\{-\left(\frac{V_i - V_e(nN_0m)}{2\Sigma}\right)^2\right\}\varphi(n,p)$$

$$I_i = \sum_{n=1}^{N}\frac{nN_0m}{(2\pi\Sigma)^{1/2}}\exp\left\{-\left(\frac{V_i - V_e(nN_0m)}{2\Sigma}\right)^2\right\}\varphi(n,p)$$

with $V_i = i\Delta V$.

In the example shown in Figure 12 we used $\Delta v = 0.2$ mL, $L = 200$, and the constant value $\Sigma = 1$ mL. The chromatograms in Figure 12 are well representative of what we obtained in real experiments (Figures 1–4), although the real linear precursor sample has a finite polydispersity. They exhibit the same qualitative features we discussed in section V.

In the final step we use the procedure described in section IV to calculate first the cumulative weight distribution function (Figure 13) and then the size distribution function (Figure 14).

In Figures 13 and 14, the points are obtained from the "experimental" values given by eq B3, and the continuous line is the input distribution function (B1). In Figure 14, (B1) should be represented as a set of δ functions, but on the scale of the figure, the 170 δ functions turn rapidly to a filled surface. Thus for convenience of the eye, we represent the set B1 as a continuous curve although it is actually discontinuous.

We see that the agreement between the calculated and the input distribution is very good except at the very ends of the distribution. For higher values of Σ ($\Sigma > 2$ mL), we found that the region where the two curves agree shrinks a little. However, the shape of the chromatograms changes drastically and no longer corresponds to our experiments. The chromatograms rather describe a different system, which we studied by the same technique. This study will be reported in a forthcoming paper.[25]

Registry No. Polystyrene, 9003-53-6.

References and Notes

(1) Flory, P. J. *Principles of Polymer Chemistry*; Cornell University Press: Ithaca, NY, 1953.
(2) de Gennes, P.-G. *Scaling Concepts in Polymer Physics*; Cornell University Press: Ithaca, NY, 1979.
(3) Dusek, K.; Prins, W. *Adv. Polym. Sci.* **1969**, *6*, 1.
(4) Bastide, J. Thèse d'Etat, 1985, Strasbourg.
(5) Candau, S.; Bastide, J.; Delsanti, M. *Adv. Polym. Sci.* **1982**, *44*, 27.
(6) Stauffer, D.; Coniglio, A.; Adam, M. *Adv. Polym. Sci.* **1982**, *44*, 103.
(7) Stockmayer, W. H. *J. Chem. Phys.* **1943**, *11*, 45.
(8) Stockmayer, W. H. *J. Chem. Phys.* **1944**, *12*, 125.
(9) Leibler, L.; Schosseler, F. *Phys. Rev. Lett.* **1985**, *55*, 1110. Leibler, L., Schosseler, F. *Physics of Finely Divided Matter*; Boccara, N., Daoud, M., Eds.; Springer Proceeding in Physics, 1985; Vol. 5.
(10) Schosseler, F.; Leibler, L. *J. Phys. Lett.* **1984**, *45*, L501. Schosseler, F.; Leibler, L. *Macromolecules* **1985**, *18*, 398.
(11) de Gennes, P.-G. *J. Phys. (Les Ulis, Fr.)* **1975**, *36*, 1049. de Gennes, P.-G. *J. Phys. Lett.* **1976**, *37*, L1. Stauffer, D. *J. Chem. Soc., Faraday Trans. 2* **1976**, *72*, 1354.
(12) Stauffer, D. *Phys. Rep.* **1979**, *54*, 1.
(13) Stauffer, D. In *On Growth and Forms*; Stanley, H. E., Ostrowsky, N., Eds.; Martinus Nijhoff: Amsterdam, 1986.
(14) Ouano, A. C.; Kaye, W. *J. Polym. Sci. Polym. Chem. Ed.* **1974**, *12*, 1151.
(15) Benoît, H.; Grubisic-Gallot, Z.; Rempp, P.; Decker, D.; Zilliox, J. G. *J. Chim. Phys.* **1966**, *63*, 1507. Grubisic-Gallot, Z.; Rempp, P.; Benoit, H. *Polym. Lett.* **1967**, *5*, 573.
(16) Gallot, Z. 9th GFP Symposium on SEC, Villeneuve d'Ascq, 1984.
(17) Zimm, B. H.; Stockmayer, W. H. *J. Chem. Phys.* **1949**, *17*, 1301.
(18) Lederer, K.; Imrich-Schwarz, G.; Dunky, M. *J. Appl. Polym. Sci.* **1986**, *32*, 4751. Kim, C. J.; Hamielec, A. E.; Benedek, A. *J. Liq. Chromatogr.* **1982**, *5*, 425; **1982**, *5*, 1277.
(19) Grubisic-Gallot, Z.; Marais, L.; Benoît, H. *J. Chem. Soc. B* **1967**, *5*, 735.
(20) de Gennes, P.-G. *C.R. Acad. Sci., Paris* **1980**, *281*, B17. Isaacson, J. I.; Lubensky, T. C. *J. Phys. Lett.* **1980**, *41*, L469. Parisi, G.; Sourlas, N. *Phys. Rev. Lett.* **1981**, *46*, 871.
(21) Daoud, M.; Joanny, J. F. *J. Phys. (Les Ulis, Fr.)* **1981**, *42*, 1359.
(22) He, X.; Lapp, A.; Herz, J. *Makromol. Chem.* **1988**, *189*, 1061.
(23) Schosseler, F.; Leibler, L.; Daoud, M.; Benoît, H., to be submitted for publication.
(24) Schmidt, M.; Burchard, W. *Macromolecules* **1981**, *14*, 370. Munch, J. P.; Ankrim, M.; Hild, G.; Okasha, R.; Candau, S. J. *Macromolecules* **1984**, *17*, 110. Candau, S.; Ankrim, M.; Munch, J. P.; Rempp, P.; Hild, G.; Okasha, R. In *Physical Optics of Dynamic Phenomena and Processes in Macromolecules Systems*; Walter de Gruyter: Berlin, 1987. Bouchaud, E.; Delsanti, M.; Adam, M.; Daoud, M.; Durand, D. *J. Phys. (Les Ulis, Fr.)* **1986**, *47*, 1273. Adam, M.; Delsanti, M.; Munch, J. P.; Durand, D. *J. Phys. (Les Ulis, Fr.)* **1987**, *48*, 1809. Collette, C.; Lafuma, F.; Audebert, R.; Leibler, L., to be submitted for publication.
(25) Lapp, A.; et al., to be submitted for publication.
(26) Bastide, J.; Marchal, J., manuscript in preparation.
(27) Chapiro, A. *High Polymers*; Wiley Interscience: New York, 1962; Vol. XV, Chapter XI.
(28) Ausloos, P.; Lias, S. G.; Rebhert, R. E. *J. Phys. Chem.* **1981**, *85*, 2322.
(29) Abraham, R. J.; Whitten, D. H. *Trans. Faraday Soc.* **1958**, *54*, 1291. Florin, R. E.; Wall, L. A.; Brown, D. W. *J. Polym. Sci.* **1963**, *1*, 101.
(30) In fact the hydrodynamic volume is proportional to $R_g^2R_H$, where R_H is the hydrodynamic radius of the molecule, but we neglect here possible dynamical crossover effects as described in ref 31. In this estimation of ν_b, they should act as a second-order correction.
(31) Weill, G.; des Cloizeaux, J. *J. Phys. (Les Ulis, Fr.)* **1979**, *40*, 99.